International Journal of Mass Spectrometry 297 (2010) 85–95

Contents lists available at ScienceDirect

International Journal of Mass Spectrometry

journal homepage: www.elsevier.com/locate/ijms

Infrared and electronic spectroscopy of p-$C_6H_4Cl_2^+$–L_n clusters with L = Ar, N_2, H_2O, and p-$C_6H_4Cl_2$

Shamik Chakraborty, Alexander Patzer, Anita Lagutschenkov, Judith Langer, Otto Dopfer*

Institut für Optik und Atomare Physik, Technische Universität Berlin, Hardenbergstrasse 36, 10623 Berlin, Germany

ARTICLE INFO

Article history:
Received 19 April 2010
Received in revised form 22 June 2010
Accepted 23 June 2010
Available online 8 July 2010

Keywords:
Aromatic cation
Dichlorobenzene
Cluster
IR spectroscopy
Electronic spectroscopy

ABSTRACT

Mass-selected clusters of the para-dichlorobenzene cation (p-$C_6H_4Cl_2^+$, pDCB$^+$) are characterized by vibrational and electronic photodissociation spectroscopy in a molecular beam expansion. Infrared (IR) spectra of pDCB$^+$–L_n with L = Ar (n = 1–7) and L = H_2O (n = 1) and $(pDCB)_2^+$–Ar_n with $n \leq 2$ are recorded in the C–H stretch range in the $^2B_{2g}$ ground electronic state of pDCB$^+$. The IR spectra with L = Ar display essentially no shift as a function of the cluster size and approximate to high accuracy the hitherto unknown IR spectra of pDCB$^+$ and its $(pDCB)_2^+$ dimer. In addition to the two IR active C–H stretch fundamentals at 3095 and 3107 cm^{-1}, several intense combination bands are detected and assigned in the 2800–3100 cm^{-1} range for pDCB$^+$. Comparison with the spectrum of neutral pDCB demonstrates structural changes upon ionization, which are consistent with the results of quantum chemical calculations performed at the B3LYP/6-311++G** level. Analysis of the photofragmentation branching ratios for pDCB$^+$–Ar_n yields a binding energy of ~550 cm^{-1} for the roughly equivalent π-bonded Ar ligands. The IR spectrum of pDCB$^+$–H_2O displays broader transitions with only minor redshifts (~5–15 cm^{-1}) due to the stronger intermolecular interaction. The C–H stretch spectrum is consistent with a π-bonded charge-dipole configuration. The IR spectrum of $(pDCB)_2^+$, as inferred from the spectrum of the Ar-tagged species, is rather different from those of pDCB$^+$ and pDCB, indicative of a charge-resonance type interaction in this homodimer cation. The electronic spectra of the B $^2B_{3u} \leftarrow X\ ^2B_{2g}$ transition near 500 nm are reported for pDCB$^+$–Ar, pDCB$^+$–N_2, and pDCB$^+$–H_2O. Only small shifts of the electronic origin transition are observed upon complexation, indicating little change in the intermolecular interaction energy upon electronic excitation. This conclusion is also supported by the modest excitation of unresolved intermolecular modes, suggesting that also the geometry changes in these clusters are small upon B ← X excitation.

1. Introduction

Aromatic molecules and their interactions with the surrounding environment are vital for chemical and biological recognition phenomena [1–3]. To understand these processes at the molecular level, a plethora of spectroscopic studies have been performed on aromatic clusters isolated in molecular beams, yielding important information about fundamental properties of the various types of their intermolecular interaction potentials [4–9]. In comparison to their neutral counterparts, spectroscopic information on aromatic cations and their clusters is more limited. Ionization has a dramatic impact on the structural, vibrational, electronic, and chemical properties of the aromatic ion and also its interaction with surrounding ligands [3–13]. Popular techniques to obtain high-resolution spectra of size-selected aromatic cluster ions are derived from resonance-enhanced multiphoton photoionization (REMPI), when combined with infrared (IR) and electronic photodissociation [3,6,13–15], or threshold ionization techniques, such as zero-kinetic-energy photoelectron spectroscopy [5,7], mass-analyzed threshold ionization (MATI) [5,8], and photoionization efficiency measurements [16]. In an alternative approach, the open-shell aromatic ions can be generated right away in an ion source, e.g., by electron impact or discharge, and then directly be probed by IR and electronic photodissociation [3,11,17–20].

The present work reports IR and electronic spectra of cold clusters of the para-dichlorobenzene cation (p-$C_6H_4Cl_2^+$, pDCB$^+$, Fig. 1a) generated in an electron impact plasma expansion source, which are obtained via photodissociation in a tandem mass spectrometer [21]. This approach has successfully been applied to record IR spectra of a variety of aromatic cluster ions [11], including benzene [3,20,22–26], several benzene derivatives (e.g., toluene [24], phenols [6,27–30], aniline [31,32], fluorobenzene [33]), substituted polycyclic aromatic ions (naphthole [34]), and heterocyclic ions (e.g., imidazole [35] and indole [36]). In combination with

* Corresponding author. Fax: +49 30 31423018.
E-mail address: dopfer@physik.tu-berlin.de (O. Dopfer).

1387-3806/$ – see front matter © 2010 Elsevier B.V. All rights reserved.
doi:10.1016/j.ijms.2010.06.026

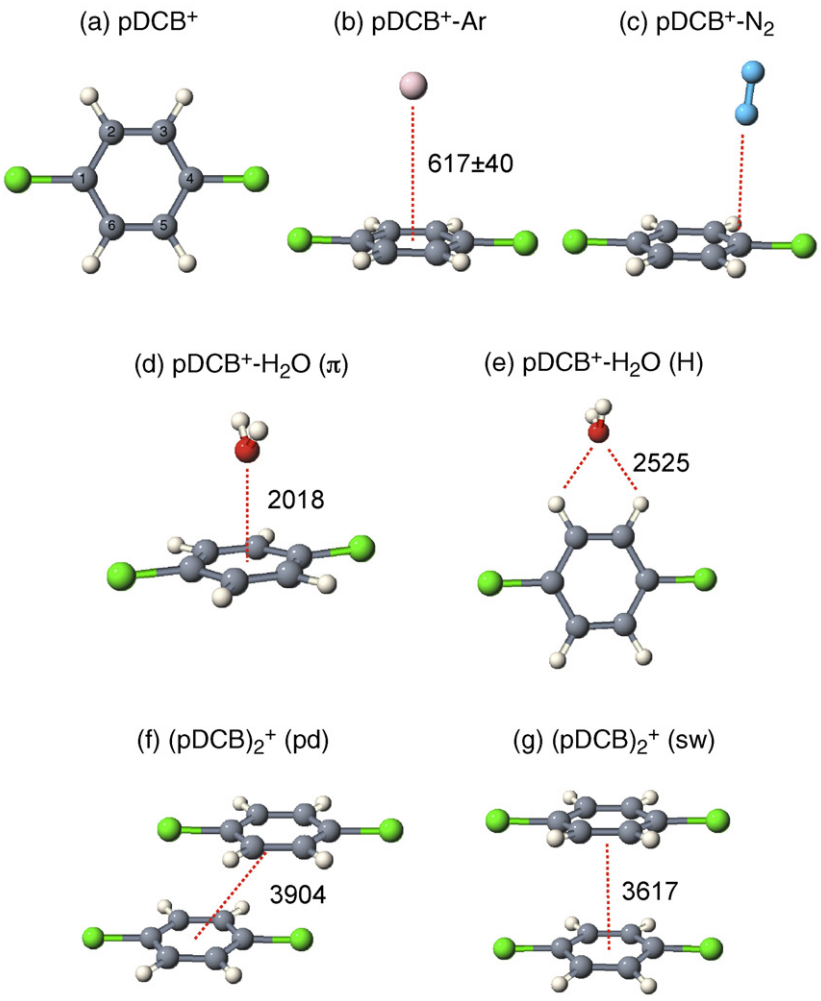

Fig. 1. Structures of $pDCB^+$ (a), $pDCB^+$–Ar (b), $pDCB^+$–N_2 (c), $pDCB^+$–H_2O (d and e), and $(pDCB)_2^+$ (f and g) obtained from B3LYP calculations. Binding energies are given in cm^{-1}. The experimental binding energy for $pDCB^+$–Ar is taken from Ref. [67].

quantum chemical calculations, these studies yielded detailed insight into fundamental properties of the intermolecular potential, such as the preferred ion-ligand binding motif (H-bonding or π-bonding), the interaction strength, and the dependence of the potential on the charge state, the substitution of functional groups, the type of ligand (polar and nonpolar), and the degree of microsolvation. More recently, this approach has been extended to electronic spectroscopy [3,20,21] in order to explore the effects of electronic excitation on the interaction of aromatic cluster ions. There are only a few ionic aromatic clusters characterized so far by electronic spectroscopy [3,15,17,20,37–42], and the spectra provide information about the effect of the charge distribution on the intermolecular potential, as well as the chemical composition and reactivity of the cluster ions.

The present work reports IR spectra of $pDCB^+$–L_n with L = Ar (n = 1–7) and H_2O (n = 1) and $(pDCB)_2^+$–Ar_n with $n \leq 2$ recorded in the C–H stretch range (2800–3200 cm^{-1}) as well as electronic spectra of the $B\,^2B_{3u} \leftarrow X\,^2B_{2g}$ transition of $pDCB^+$–L with L = Ar, N_2, and H_2O in the 500 nm range. The IR spectra of $pDCB^+$–Ar_n provide a first impression of $pDCB^+$ microsolvated in a nonpolar solvent. The spectra are independent of the degree of Ar solvation and yield for the first time experimental information about the C–H stretch frequencies of bare $pDCB^+$. It turns out that, in contrast to related aromatic ions [22,24,35,43–45], the $pDCB^+$ spectrum in this spectral range is heavily complicated by the occurrence of a variety of intense combination bands. Their assignment required a detailed quantum chemical study of the structural and vibrational properties of $pDCB^+$ in its $^2B_{2g}$ ground electronic state, which gave rise to a substantial reassignment of modes in the fingerprint range identified previously by IR, Raman, and MATI spectroscopy [46–48]. Comparison with the corresponding data of neutral pDCB [46,49–53] reveals the effects of ionization on the structural and vibrational properties of pDCB. The analysis of recent IR spectra of $pDCB^+$–$(H_2O)_n$ with n = 1 and 2 in the O–H stretch range demonstrated that microhydration of $pDCB^+$ proceeds along two competing routes, namely interior ion solvation and the formation of a hydration network with $pDCB^+$ on the surface [21]. The $pDCB^+$–H_2O spectrum is consistent with a charge-dipole structure, although the exact binding site of H_2O (H-bonding or π-bonding, Fig. 1) could not be established from the O–H stretch spectrum by comparison with quantum chemical calculations. The present analysis of the C–H stretch range is indicative of the observation of a π-bonded isomer. Homodimers of aromatic cations are interesting molecular species, as they may have either symmetric configurations (e.g., benzene [37,54–56]), giving rise to strongly-bound charge-resonance structures featuring the onset of chemical bonding, or asymmetric geometries, leading to electrostatically bound ion-neutral complexes (e.g., phenol [6,7,57]). Although no spectroscopic, mass spectrometric, and theoretical information appears to be available for $(pDCB)_2^+$, it probably adopts a charge-resonance structure in its ground electronic state, similar to the related homodimer cations of benzene, $(Bz)_2^+$ [37,56], and para-difluorobenzene, $(pDFB)_2^+$

[58,59]. For the latter complexes, low-lying electronic transitions in the photodissociation spectra confirmed that they have symmetric sandwich-type geometries with equivalent monomer units equally sharing the positive charge [37,58]. Their relatively high binding energies of 0.65–0.9 eV [54,60–62] and 0.7 eV [58] confirm this view. Due to their large binding energy, IR photodissociation spectra of aromatic homodimer cations are usually broad and unstructured [17]. The present $(pDCB)_2^+$–Ar_n spectra provide for the first time a highly resolved IR spectrum of a cold aromatic homodimer cation, offering the opportunity to analyze the effects of the charge-resonance on the vibrational spectrum. Comparison of the electronic spectra of the B ← X transition of the $pDCB^+$–L dimers with L = Ar, N_2, and H_2O [21] with the monomer spectrum [63] unravels the effects of microsolvation of $pDCB^+$ with polar and nonpolar ligands on its electronic structure. At the same time, it provides information on the effect of electronic excitation on the intermolecular interaction.

Previous spectroscopic work on the vibrational properties in the $^2B_{2g}$ ground electronic state of $pDCB^+$ relevant for the present work is available from MATI [64] and photoelectron spectroscopy in the gas phase [65], as well as IR and Raman spectra in rare gas matrices [46,47]. The high-resolution vibronic spectrum of the B ← X transition of $pDCB^+$ was recently recorded via two-photon dissociation in a cryogenic ion trap [63]. The assignments of the electronically excited states was confirmed by recent high-level ab initio calculations [66]. Previous spectroscopic and theoretical information about $pDCB^+$–L dimers is restricted to the recent IR and electronic spectra of $pDCB^+$–H_2O discussed above [21], as well as a MATI spectrum of $pDCB^+$–Ar [67]. The latter provides a binding energy of $D_0 = 617 \pm 40\,cm^{-1}$ for $pDCB^+$–Ar in the $^2B_{2g}$ ground state and is indicative of a π-bound equilibrium structure with C_{2v} symmetry (Fig. 1b). Vibrational frequencies and assignments for neutral pDCB are available from IR and Raman spectroscopy [46,49–53].

2. Experimental and theoretical methods

IR and electronic photodissociation spectra of $pDCB^+$–Ar_n, $(pDCB)_2^+$–Ar_n, $pDCB^+$–N_2, and $pDCB^+$–H_2O clusters are recorded in a tandem quadrupole mass spectrometer coupled to an electron impact ionization source and an octopole ion guide [11,68]. The weakly bound clusters are generated in a pulsed supersonic plasma expansion by electron and/or chemical ionization of pDCB close to the nozzle orifice and subsequent clustering reactions in the high pressure regime of the expansion [21]. The expanding gas mixture is produced by passing either Ar or N_2 buffer gas at 5–10 bar stagnation pressure through a reservoir filled with pDCB heated to ~320 K. pDCB has been purchased from Aldrich (≥99% purity). To generate $pDCB^+$–H_2O, the carrier gas is passed through a reservoir filled with water at room temperature before entering the pDCB reservoir [21]. The typical working pressure in the source chamber and in the octopole ion trap are 10^{-5} and 10^{-8} mbar, respectively.

A typical mass spectrum of the ion source using Ar carrier gas is shown in Fig. 2 for the mass range 10–450 u. The mass spectrum is dominated by X^+–Ar_n cluster series with X = Ar, pDCB, $(pDCB)_2$, and H_2O. The asterisks indicate the major fragment ions of $pDCB^+$ upon electron ionization, corresponding to the loss of one and two Cl atoms [69]. The assignment of the mass peaks containing pDCB molecules are confirmed by the characteristic isotope pattern expected for the natural abundance of ^{35}Cl and ^{37}Cl of 76 and 24%, respectively. Only the monoisotopic $(pDCB)_p^+$–L_n clusters ($p = 1, 2$) were studied spectroscopically and theoretically. In general, the abundance of $pDCB^+$–L_n clusters decreases rapidly with increasing cluster size, consistent with the formation of weakly bound clusters by sequential addition of individual ligands to the molecular ion [11,30]. For example, although the relative intensities of $pDCB^+$–Ar_n

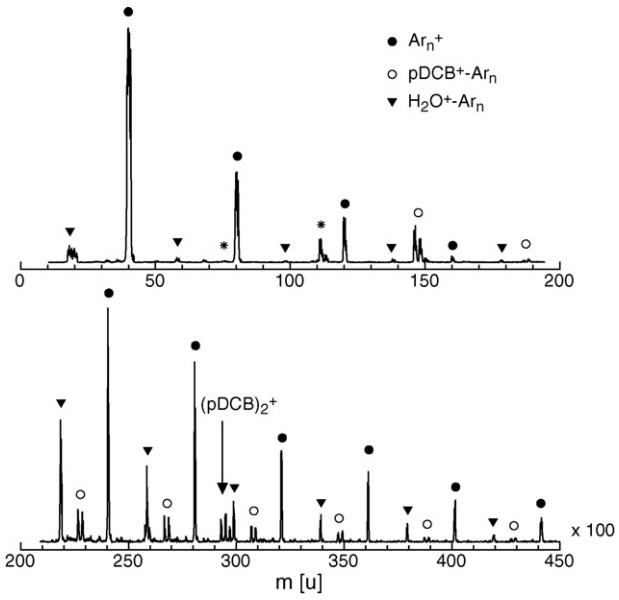

Fig. 2. Mass spectrum of the electron impact cluster ion source for an expansion of pDCB in 7 bar Ar. Major peaks are assigned to the X^+–Ar_n cluster series with X = Ar, pDCB, and H_2O. The arrow indicates the peak of $(pDCB)_2^+$. The asterisks indicate the major fragment ions of $pDCB^+$ upon electron ionization, corresponding to the loss of one and two Cl atoms. The spectrum in the lower trace is vertically expanded by a factor of 100.

with $n = 1$ and $n = 7$ in Fig. 2 are only 5 and 0.05% of that of $pDCB^+$, respectively, IR spectra with respectable signal-to-noise ratios can be obtained for these clusters, demonstrating the high sensitivity of the experimental approach.

The $pDCB^+$–L_n ions of interest are mass selected by the first quadrupole and irradiated in an adjacent octopole with a tunable laser pulse. The latter is generated by an IR optical parametric oscillator (IR-OPO) or by a dye laser to record IR or electronic spectra, respectively [21]. Both lasers were pumped by a Q-switched nanosecond Nd:YAG laser. The IR-OPO laser is characterized by a pulse energy of ~10 mJ in the 2700–3300 cm^{-1} range, a repetition rate of 10 Hz, and a bandwidth of 1 cm^{-1}. Calibration of the IR laser frequency is accomplished by comparing atmospheric water absorptions along the IR laser path with the published spectrum [70]. The dye laser is operated at 20 Hz with Coumarin 307 and calibrated with a wavemeter. The typical pulse energy employed is of the order of 1 mJ. Resonant excitation into vibrational or vibronic resonances induced evaporation of one or several ligands, according to:

$$pDCB^+\text{–}L_n + h\nu \rightarrow pDCB^+\text{–}L_m + (n-m)L \quad (1)$$

$$(pDCB)_2^+\text{–}Ar_n + h\nu \rightarrow (pDCB)_2^+ + nAr \quad (2)$$

In the case of vibrational excitation, the rupture of the weak intermolecular bonds is the only fragment channel observed. For electronic excitation of $pDCB^+$–L, also fragment ions of $pDCB^+$ are detected as a minor channel. The generated fragment ions are selected by the second quadrupole and monitored as a function of the laser frequency to obtain the IR and electronic photodissociation spectra of the corresponding parent clusters. As an example, Fig. 3 shows the mass spectra obtained by mass selecting $pDCB^+$–Ar_4 ($m = 306$ u) with the first quadrupole and scanning the second one without excitation (a), with resonant IR excitation at 3107 cm^{-1} (b), and with collisional activation (c). For the latter process, the octopole is filled with N_2 up to 10^{-5} mbar, which results in collisions with ~10 eV collision energy in the laboratory frame. The mass spectrum (a) reveals little fragmentation into the $m = 3$ fragment channel arising from metastable decay (MD) of

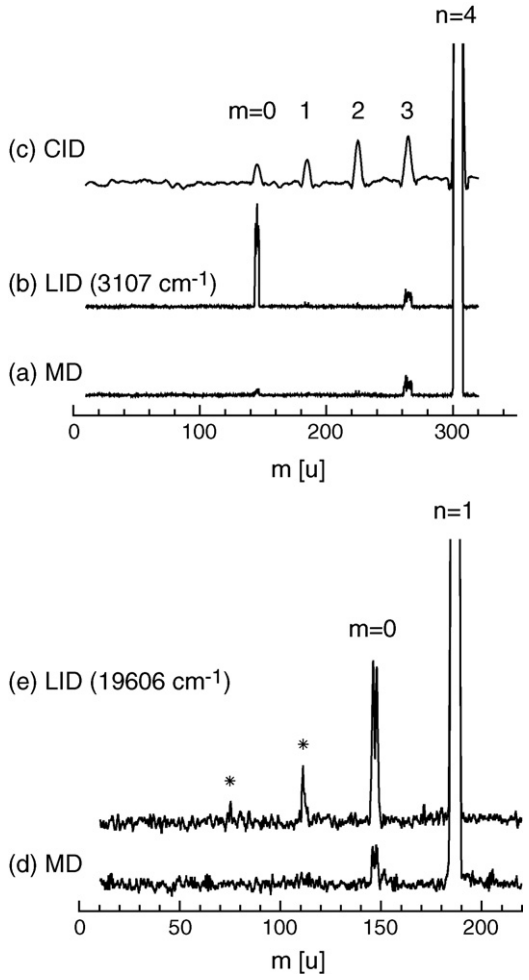

Fig. 3. Mass spectra obtained by mass selecting $pDCB^+–Ar_4$ (m = 306 u) with the first quadrupole and scanning the second one without excitation (a), with resonant IR excitation at 3107 cm^{-1} (b), and with collisional activation (c). The mass spectrum (a) reveals fragmentation into $pDCB^+–Ar_m$ with m = 0–3 arising from metastable decay (MD), whereas spectra (b) and (c) display additional fragmentation arising from laser-induced (LID) or collision-induced dissociation (CID), respectively. Mass spectra (d) and (e) are obtained by mass selecting $pDCB^+–Ar$ (m = 186 u) with the first quadrupole and scanning the second one without excitation and with resonant electronic excitation at 19,606 cm^{-1}, respectively. The asterisks indicate fragment ions with m = 111 and 76 u arising from to the elimination of one and two Cl atoms from $pDCB^+$.

hot n = 4 parent clusters in the octopole region. Spectra (b) and (c) display additional fragmentation arising from laser-induced (LID) or collision-induced dissociation (CID), respectively. Both the LID and the CID fragments arise from the loss of up to all four Ar ligands and confirm the identification of the m = 306 u mass peak as $pDCB^+–Ar_4$. However, there is a qualitative difference between the LID and CID spectra of $pDCB^+–Ar_n$. While collisions generate a broad distribution of fragment ions (here m = 0–3), LID leads to a narrow range of fragment channels (here only m = 0). The latter information can be used to estimate the binding energies of the ligands (*vide infra*). Fig. 3 also shows the mass spectra obtained by mass selecting $pDCB^+–Ar$ (m = 186 u) with the first quadrupole and scanning the second one without excitation (d) and with resonant electronic excitation at 19,606 cm^{-1} (e), respectively. In contrast to IR excitation in the ground electronic state, electronic excitation can also induce dissociation of $pDCB^+$ via absorption of more than one photon [63], leading to fragment ions with m = 111 and 76 u, corresponding to the loss of one and two Cl atoms, respectively [69]. To separate the contribution of MD from that of LID, the ion source is triggered at twice the laser frequency, and signals from alternating triggers are subtracted. This procedure compensates for slow variations of parent ion currents generated in the ion source. Although the IR spectra are not normalized for laser intensity fluctuations, the relative intensities of widely spaced bands are believed to be accurate to within a factor of two, mainly due to the changes in the spatial overlap between the IR laser and ion beams.

The geometry and vibrational frequencies of pDCB, $pDCB^+$, and $(pDCB)_2^+$ are characterized at the B3LYP/6-311++G** level [71] in order to support the vibrational assignment and to investigate the effects of ionization and dimerization on the structure and the IR spectrum. Harmonic frequencies are scaled by a factor of 0.9656 and 0.9824 for frequencies above and below 2000 cm^{-1}, respectively, to optimize the agreement between the calculated and the measured frequencies of $pDCB^+$ (*vide infra*) [46,48]. Such a dual scaling factor procedure accounts for the rather different anharmonicity of hydrid stretch modes and skeletal vibrations in the fingerprint range [72]. Calculations at the UMP2 level yielded several unrealistic vibrational frequencies and IR intensities for $pDCB^+$, probably arising from significant spin contamination. The failure of the UMP2 method for $pDCB^+$ prevented reliable calculations for the $pDCB^+–Ar$ and $pDCB^+–N_2$ interaction. As dispersion forces are relevant for this interaction, also the B3LYP technique is not suitable. Consequently, reliable calculations have been restricted to pDCB, $pDCB^+$, and the $(pDCB)_2^+$ dimer.

3. Results and discussion

3.1. Infrared spectra

3.1.1. $pDCB^+–Ar_n$

Fig. 4 compares the IRPD spectra of $pDCB^+–Ar_n$ recorded in the C–H stretch range by monitoring the $pDCB^+–Ar_m$ channel (indicated as $n \rightarrow m$). All spectra are similar in appearance in terms of band positions, band shapes, and widths. In total, eight transitions, labeled A–H, are readily observed in the spectral range investigated, 2750–3250 cm^{-1}. The positions and suggested vibrational assign-

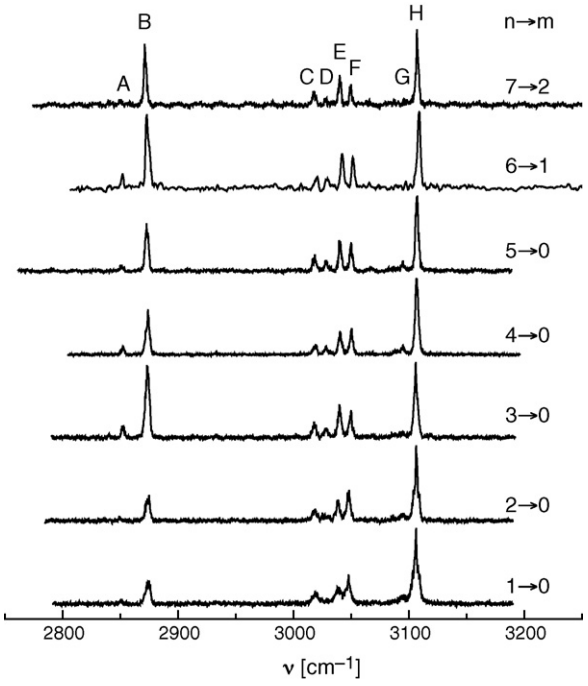

Fig. 4. IRPD spectra of $pDCB^+–Ar_n$ recorded in the dominant $pDCB^+–Ar_m$ fragment channel (indicated as n → m). The positions and assignments of the transitions observed (A–H) are listed in Table 1.

Table 1
Positions (in cm^{-1}) and suggested assignments of the transitions (A–K) observed in the IR spectra of $pDCB^+$–Ar and $pDCB^+$–H_2O (Figs. 4 and 7).[a].

		A	B	C	D	E	F	K	G	H
L = Ar	ν [cm^{-1}]	2851	2874	3019	3029	3038	3047		3095	3107
L = H_2O	ν [cm^{-1}]	2845	2868	3015	n.r.[b]	3033	3038	3067	3086	3102
	Assignment	$\nu_{11}+\nu_{24}$ = 2849	$\nu_{19}+\nu_{24}$ = 2872 $\nu_2+\nu_{20}$ = 2910	$\nu_2+\nu_{19}$ = 3067 $\nu_2+\nu_{11}$ = 3044 $\nu_{11}+\nu_{12}+\nu_{29}$ = 3020 $2\nu_{12}+\nu_{28}$ = 3024 $\nu_2+\nu_6+\nu_{11}$ = 3033						ν_{10}	ν_{18}

[a] A detailed list of all peak positions of $pDCB^+$–Ar_n with n = 1–7 is available in Table T1 in Supporting Information.
[b] Not resolved.

ments are listed in Table 1. The vibrational frequencies are nearly independent of the cluster size n, with differences of less than $\pm 4\,cm^{-1}$ in the size range investigated ($n \leq 7$). Moreover, the relative IR intensities for most of the transitions are very similar (*vide infra*). As Ar solvation has essentially no impact on the IR spectrum of $pDCB^+$, the $pDCB^+$–Ar_n spectra provide a very good approximation to the IR spectrum of the bare ion in its ground electronic state (messenger technique [14,24,26,73]). The observed features must clearly be attributed to intramolecular vibrational modes of $pDCB^+$ and cannot arise from other sources, including intermolecular vibrations and rotational or other substructure (band heads, etc.). The width of the transitions is typically 2–4 cm^{-1} and attributed to a combination of unresolved rotational substructure and the limited laser bandwidth ($\sim$1 cm^{-1}). As a general trend, the widths decrease slightly with increasing n, as the larger clusters are slightly colder and have smaller rotational constants [74–76]. Although the IR spectra of $pDCB^+$–Ar_n do not provide any information about their structure, the dimer is supposed to have a π-bonded geometry with C_{2v} symmetry (Fig. 1b) [67], and larger clusters are derived by further solvation of $pDCB^+$ above and below the aromatic plane.

The planar $pDCB^+$ cation has D_{2h} symmetry in its $^2B_{2g}$ ground electronic state. Thus, only two out of the four possible C–H stretch fundamentals are IR active (*vide infra*), and these are expected to provide the only contribution to the IR spectrum in the spectral range investigated in the harmonic oscillator approximation. However, the experimental $pDCB^+$ spectrum displays as many as eight transitions with measurable IR intensity. In this respect, the IR spectrum of $pDCB^+$ is more complex than those of related aromatic cations, e.g., benzene$^+$ [22,24,26,43], fluorobenzene$^+$ [33] or protonated benzene derivatives [19,44,45,77–81].

In order to aid the vibrational assignments, the geometry and vibrational spectrum of $pDCB^+$ have been calculated at the B3LYP/6-311++G** level. To unravel the effects of ionization on the structure and vibrational frequencies, the corresponding data of the neutral species are also evaluated at the same theoretical level. Table 2 summarizes the structural parameters obtained for $pDCB^+$ and pDCB in their ground electronic states. Table 3 lists all calculated fundamental frequencies of $pDCB^+$ and pDCB, along with their symmetry species and IR intensity, as well as experimental frequencies available from IR, Raman, and MATI spectra [46,48]. We employ the Mulliken notation for normal modes and the transformation to the alternative Wilson notation may, for example, be found in Ref. [48]. $pDCB^+$ has D_{2h} symmetry and, with the z-axis passing through the Cl atoms and the x-axis being perpendicular to the molecular plane, the symmetry species of the 30 normal modes transform according to $6a_g + b_{1g} + 3b_{2g} + 5b_{3g} + 2a_u + 5b_{1u} + 5b_{2u} + 3b_{2u}$ [51]. The normal modes can be classified in four C–H stretches, in-plane and out-of-plane bends ($4\sigma_{CH}$, $4\beta_{CH}$, $4\gamma_{CH}$), two C–Cl stretches, in-plane and out-of-plane bends ($2\sigma_{CCl}$, $2\beta_{CCl}$, $2\gamma_{CCl}$), four C–C and ring stretches ($4\sigma_{CC}$ 4 ring), and one in-plane and two out-of-plane C–C bends (β_{CC}, $2\gamma_{CC}$). The IR allowed vibrations are those with b_{1u}, b_{2u}, and b_{3u} symmetry, i.e. the fundamentals ν_{10}–ν_{14}, ν_{18}–ν_{22}, and ν_{28}–ν_{30}. Raman active vibrations are those with gerade symmetry, i.e. the fundamentals ν_1–ν_6, ν_9, ν_{15}–ν_{17}, and ν_{23}–ν_{27}. The vibrations accessible by MATI spectroscopy depend on the choice of the intermediate state [48].

pDCB has the electronic configuration $\cdots (3b_{3u})^2(1b_{1g})^2(3b_{2g})^2(11a_g)^0(7b_{2u})^0 \cdots$ in its ^1A_g ground electronic state and ionization corresponds to removal of an electron from a bonding aromatic π-orbital of b_{2g} symmetry, leading to the $^2B_{2g}$ ground electronic state of $pDCB^+$. As noted previously [48,64,66], ionization induces a significant contraction of the C–Cl bonds (C1–Cl), an elongation of the adjacent C–C bonds (C1–C2), and a contraction of the next C–C bonds (C2–C3), leading to an overall expansion of the aromatic ring (see Fig. 1a for the atom numbering). At the same time, the C–H bonds slightly elongate on ionization (Table 2).

The structural changes induced by ionization directly translate into modifications of the vibrational frequencies. For example, the σ_{CCl} frequencies ν_6 and ν_{14} increase due to the contraction of the C-Cl bonds. In addition, the σ_{CC} frequencies involving stretching of the C1–C2 and C4–C5 bonds (ν_{11}, ν_{24}) substantially drop in frequency, whereas those involving stretching of the C2–C3 and C5–C6 bonds (ν_2, ν_{19}) increase significantly. Interestingly, all C–H stretch frequencies increase upon ionization by 8–12 cm^{-1}, although the C–H bonds get slightly longer. This apparent inconsistency is rationalized by a simultaneous change in the HCC bond angles by 1°, leading to a slight Duschinsky rotation of the normal coordinates.

As the Ar ligands interact only weakly with $pDCB^+$, the same (near) symmetry group and selection rules as for the $pDCB^+$ monomer (D_{2h}) are also applied for $pDCB^+$–Ar_n. The fact that the IR spectra of $pDCB^+$–Ar_n in Fig. 4 are quite independent of the

Table 2
Structural parameters (distances in Å, angles in degrees) of $pDCB^+$, pDCB, and $(pDCB)_2^+$ in their ground electronic states evaluated at the B3LYP/6-311++G** level (Fig. 1).

	C1–Cl	C1–C2	C2–C3	Ring[a]	C1–H	C1C2C3	C6C1C2	HC2C3
$pDCB^+$ ($^2B_{2g}$)	1.6931	1.4228	1.3689	8.4290	1.0826	119.3	121.4	121.1
pDCB (^1A_g)	1.7567	1.3914	1.3928	8.3512	1.0824	119.5	121.0	120.3
Δ[b]	−0.0636	+0.0314	−0.0239	+0.0778	+0.0002	−0.2	+0.4	+0.8
$(pDCB)_2^+$ (pd)	1.7247	1.4073	1.3806	8.3910	1.0824	119.4	121.2	120.7
	1.7204	1.4076			1.0824		121.1	120.7
$(pDCB)_2^+$ (sw)	1.7223	1.4070	1.3807	8.3894	1.0825	119.4	121.1	120.7

[a] Circumference of carbon ring.
[b] Difference upon ionization.

Table 3
Calculated and experimental vibrational frequencies (in cm^{-1}) of $pDCB^+$ and pDCB in their ground electronic states evaluated at the B3LYP/6-311++G** level.

Symmetry	Mulliken	Mode	$pDCB^+$	$pDCB^+$	pDCB	pDCB	Δ^g	Δ^g
			B3LYP[a]	Exp	B3LYP[a]	Exp[e]	B3LYP	Exp
a_g	ν_1	σ_{CH}	3108 (0)		3099 (0)	3072	+9	
	ν_2	σ_{CC}	1606 (0)	1598[c]	1586 (0)	1574	+20	+24
	ν_3	β_{CH}	1201 (0)	1189[c]	1176 (0)	1169	+25	+20
	ν_4	Ring	1096 (0)	1113[c]	1081 (0)	1096	+15	+17
	ν_5	Ring	754 (0)	758[b]	741 (0)	747	+13	+11
	ν_6	σ_{CCl}	330 (0)	334[b], 330[c]	323 (0)	328	+7	+6, +2
a_u	ν_7	γ_{CH}	979 (0)		951 (0)	951	+28	
	ν_8	β_{CC}	360 (0)	357*[,b]	412 (0)	405	−52	−48
b_{1g}	ν_9	γ_{CH}	786 (0)		809 (0)	815	−23	
b_{1u}	ν_{10}	σ_{CH}	3097 (6)	3095[d]	3085 (1)	3078	+12	+17
	ν_{11}	σ_{CC}	1438 (227)	1429[c]	1479 (109)	1477	−41	−48
	ν_{12}	Ring	1097 (290)	1110[c]	1081 (112)	1090	+16	+20
	ν_{13}	β_{CH}	984 (17)	986[c]	1007 (62)	1015	−23	−29
	ν_{14}	σ_{CCl}	568 (45)		530 (41)	550	+38	
b_{2g}	ν_{15}	γ_{CH}	963 (0)		935 (0)	934	+28	
	ν_{16}	γ_{CC}	676 (0)		713 (0)	687	−37	
	ν_{17}	γ_{CCl}	239 (0)		291 (0)	298	−52	
b_{2u}	ν_{18}	σ_{CH}	3106 (32)	3107[d]	3098 (1)	3087	+8	+20
	ν_{19}	σ_{CC}	1461 (40)		1394 (6)	1394	+67	
	ν_{20}	σ_{CC}	1304 (10)		1283 (0)	1220	+21	
	ν_{21}	β_{CH}	1123 (8)		1105 (6)	1107	+18	
	ν_{22}	β_{CCl}	231 (2)	218*[,b]	217 (1)	226	+14	−8
b_{3g}	ν_{23}	σ_{CH}	3097 (0)		3086 (0)	3065	+11	
	ν_{24}	σ_{CC}	1411 (0)		1584 (0)	1577	−173	
	ν_{25}	β_{CH}	1264 (0)		1294 (0)	1290	−30	
	ν_{26}	Ring	581 (0)	573[b]	629 (0)	626	−48	−53
	ν_{27}	β_{CCl}	356 (0)	354[b]	352 (0)	350	+4	+4
b_{3u}	ν_{28}	γ_{CH}	830 (63)	843[c]	814 (59	819	+16	+24
	ν_{29}	γ_{CC}	485 (15)	422*[,b,f]	489 (18)	485	−4	
	ν_{30}	γ_{CCl}	81 (1)		99 (0)	122	−18	

[a] IR intensities (in km/mol) are listed in parentheses.
[b] Frequencies from MATI spectra are taken from Ref. [48]. Frequencies marked by an asterisk are derived from first overtones.
[c] Raman (ν_2, ν_3, ν_4, ν_6) and IR frequencies (ν_{11}, ν_{12}, ν_{13}, ν_{28}) in an Ar matrix are taken from Ref. [46]. The 986 cm^{-1} mode is reassigned from ν_{21} to ν_{13}. The 1110 cm^{-1} mode is reassigned from ν_{13} to ν_{12}.
[d] Frequencies from IR spectrum of $pDCB^+$–Ar (present work).
[e] Taken from a compilation in Ref. [46].
[f] Probably wrong assignment (see text).
[g] Difference upon ionization.

number of Ar ligands supports this conclusion, although minor intensity variations of some bands (e.g., A and D) may be due to small effects induced by symmetry reduction upon complexation. Fig. 5 compares the experimental IR spectrum of $pDCB^+$–Ar_5 in the C–H stretch range with that calculated for $pDCB^+$ at the B3LYP level. The $pDCB^+$–Ar_5 spectrum has been chosen, as it resembles closely the one of $pDCB^+$ and displays the best signal-to-noise ratio. Fig. 5 also compares the $pDCB^+$–Ar_5 spectrum with that of pDCB taken from the NIST database [53], as an IR spectrum of pDCB measured in a molecular beam appears not to be available. While the $pDCB^+$–Ar_5 spectrum approximates a cold $pDCB^+$ spectrum, the latter one is taken in an absorption cell at room temperature leading to much broader bands.

The four C–H stretch fundamentals σ_{CH} of $pDCB^+$ are $\nu_1(a_g)$, $\nu_{10}(b_{1u})$, $\nu_{18}(b_{2u})$, and $\nu_{23}(b_{3g})$ with calculated frequencies of 3108, 3097, 3106, and 3097 cm^{-1}, respectively. They occur all in a narrow frequency interval of 11 cm^{-1}. Moreover, only ν_{10} and ν_{18} are IR active with calculated intensities of 6 and 32 km/mol, respectively. Inspection of Fig. 5 suggests that the experimental transitions H and G occurring at 3107 and 3095 cm^{-1} should be assigned to ν_{18} and ν_{10}, respectively, on the basis of the excellent agreement of their frequencies and relative IR intensities with the theoretical predictions. In fact, as these assignments have been used to derive the scaling factor of 0.9656 for the C–H stretch modes, the agreement of the frequencies may not be surprising. On the other hand, the calculations predict a blueshift of ~10 cm^{-1} for all σ_{CH} modes upon ionization, in good agreement with the experimental shifts of ~20 cm^{-1} (Fig. 5 and Table 3). Moreover, the C–H stretch frequencies of $pDCB^+$ are close to the single C–H stretch band observed for

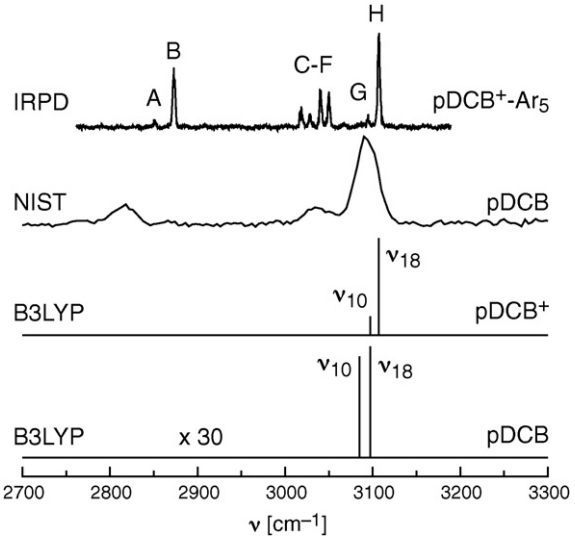

Fig. 5. IRPD spectrum of p-DCB^+–Ar_5 in the C–H stretch range (Table 1) compared to the IR absorption spectrum of neutral pDCB (Ref. [53]) and IR stick spectra of $pDCB^+$ and pDCB calculated at the B3LYP/6-311++G** level. The latter one is vertically expanded by a factor of 30. While the $pDCB^+$–Ar_5 spectrum approximates a cold $pDCB^+$ spectrum, the pDCB spectrum was recorded in an absorption cell at room temperature leading to broader bands.

$C_6H_6^+$ near 3095 cm^{-1} [26], indicating that double Cl substitution in para position has little impact on the C–H bond properties of the aromatic cation. Finally, it is noted that the intensities of the IR active C–H stretch modes of the $pDCB^+$ radical cation are much higher (up to a factor 30) than those of the neutral molecule (Fig. 5 and Table 3).

The assignment of the transitions A–F in the 2850–3050 frequency range of the IR spectra of $pDCB^+$–Ar_n cannot be to C–H stretch fundamentals. They are rather due to combination bands of skeletal ring modes. It was noted previously [50] that also the IR spectrum of neutral pDCB is complicated in the C–H stretch range by such transitions, as is evidenced by the NIST spectrum reproduced in Fig. 5. However, a firm assignment of the IR spectrum of pDCB in this frequency range is not available. Moreover, if available it cannot readily be transferred to the cation spectrum due to the changes in frequencies and IR intensities upon ionization. Thus, in an effort to derive reasonable assignments for these transitions, we considered the theoretical frequencies and IR intensities for $pDCB^+$, along with appropriate symmetry selection rules and experimentally available data. In order to determine a suitable scaling factor for the skeletal modes with frequencies below 2000 cm^{-1}, which is required for an accurate prediction of combination bands, we fitted the harmonic frequencies calculated at the B3LYP level to experimental ones available from IR, Raman, and MATI spectroscopy [46,48] in a linear regression. This fit yields a scaling factor of 0.9824, which produces deviations of less than 17 cm^{-1} between scaled and experimental frequencies for 13 modes. In order to achieve this result, we had to substantially modify the previous vibrational assignments of $pDCB^+$ by reassigning two IR active modes (ν_{12}, ν_{13}) and rejecting one assignment from MATI spectroscopy (ν_{29}). Szczepanski et al. [46] observed four IR fundamentals of $pDCB^+$ in an Ar matrix at 843, 986, 1110, and 1429 cm^{-1} and assigned them to ν_{28}, ν_{21}, ν_{13}, and ν_{11} on the basis of ROHF/6-31G calculations. Inspection of Table 3 reveals that the assignments of the 986 and 1110 cm^{-1} bands must be changed to ν_{13} and ν_{12} on the basis of the present higher-level calculations. This reassignment is much more consistent with the calculated IR intensities and reduces the frequency errors drastically from 137 and 126 cm^{-1} to 2 and 13 cm^{-1}, respectively, which are compatible with the errors for the other fundamentals (<17 cm^{-1}). Finally, the large discrepancy between the calculated frequency for ν_{29} and the value derived from the MATI spectrum (485 and 422 cm^{-1} [48]) suggests that this assignment is also incorrect.

In a first step, it seems reasonable to try an assignment of the six bands A–F to combination bands involving only two vibrational quanta [50]. The only possibilities with the correct symmetry are the following five combination bands involving two quanta of various C–C stretch modes (σ_{CC}), namely $\nu_2+\nu_{19}(b_{2u})=3067\ cm^{-1}$, $\nu_2+\nu_{11}(b_{1u})=3044\ cm^{-1}$, $\nu_2+\nu_{20}(b_{2u})=2910\ cm^{-1}$, $\nu_{19}+\nu_{24}(a_g)=2872\ cm^{-1}$, and $\nu_{11}+\nu_{24}(b_{1u})=2849\ cm^{-1}$. The latter theoretical frequencies ignore cross anharmonicities, which probably will slightly reduce the frequencies. Besides being in the correct frequency range, the C–C stretch modes are bound to couple and at least one of the two components is a strongly IR active fundamental. On the basis of their calculated frequencies, bands A and B at ~2850 and ~2875 cm^{-1} are assigned to $\nu_{11}+\nu_{24}$ and $\nu_{19}+\nu_{24}$ (or possibly $\nu_2+\nu_{20}$), respectively. Furthermore, two of the four bands C–F between 3020 and 3050 cm^{-1} are attributed to $\nu_2+\nu_{11}$ and $\nu_2+\nu_{19}$, respectively. The other two transitions must involve combination or overtone bands, involving at least three quanta. Two such combinations involving only IR active fundamentals are, for example, $2\nu_{12}+\nu_{28}(b_{3u})=3024\ cm^{-1}$ and $\nu_{11}+\nu_{12}+\nu_{29}(b_{3u})=3020\ cm^{-1}$. One option for a further triple is $\nu_2+\nu_6+\nu_{11}(b_{1u})=3033\ cm^{-1}$. A firm assignment of these transitions requires, however, a reliable prediction of the IR intensity of overtone and combination bands [82,83], which is clearly beyond the scope of the present work.

Table 4
Photofragmentation branching ratios (%) of $pDCB^+$–Ar_n clusters dissociating into $pDCB^+$–Ar_m for the two vibrational resonances at around 2874 and 3107 cm^{-1} (bands B and H).

n	Band	m = 0	m = 1	m = 2	m = 3
1–4	H	100	0	0	0
	B	100	0	0	0
5	H	100	0	0	0
	B	80	20	0	0
6	H	40	60	0	0
	B	0	100	0	0
7	H	0	30	60	10
	B	0	0	100	0

The photofragmentation branching ratios of $pDCB^+$–Ar_n clusters obtained by resonant excitation at 3110 and 2880 cm^{-1} are summarized in Table 4. The 3110 cm^{-1} transition (band H) is assigned to the C–H stretch fundamental ν_{18}, whereas the 2880 cm^{-1} transition (band B) is attributed to a combination of intramolecular C–C stretch modes, probably $\nu_{19}+\nu_{24}$. According to Eq. (1), several fragment channels m are possible for $n>1$, and the ratio sensitively depends on the cluster size and the photon energy. Previous studies on related cluster ions using the present experimental setup demonstrated that, for a given parent cluster isomer, the range of observed fragment channels is rather narrow, i.e. fragment ions are observed in one or two dominant fragment channels [11,68,84–86]. This conclusion also holds for $pDCB^+$–Ar_n (Fig. 6 and Table 4). For example, excitation of $pDCB^+$–Ar_6 at 2880 cm^{-1} (band H) produces exclusively $pDCB^+$–Ar fragments (loss of 5 Ar ligands), whereas excitation at the slightly higher-frequency transition at 3110 cm^{-1} (band H) generates 30% $pDCB^+$ and 70% $pDCB^+$–Ar, leading to the average loss of 5.3 Ar ligands. The information on the branching ratios can be used to roughly estimate the ligand binding energies, assuming a simple statistical model for the evaporation process after IR excitation, which is based on the following approximations [11]. (1) The absorbed photon energy ($h\nu_{IR}$) is available for ligand evaporation from the cluster ion. (2) All ligands are assumed to be equivalent with roughly the same dissociation energy. (3) The kinetic energy release as well as the difference in the internal energies of the parent and respective daughter clusters are neglected. (4) Only single ligands are evaporated and no larger oligomers. $pDCB^+$–Ar_n clusters up to $n=5$ eliminate all five ligands upon LID. Moreover, excitation of $pDCB^+$–Ar_6 and $pDCB^+$–Ar_7 at 2880 cm^{-1} is sufficient to eliminate 5 but not 6 Ar ligands. This observation yields an average binding energy of $530\pm50\ cm^{-1}$

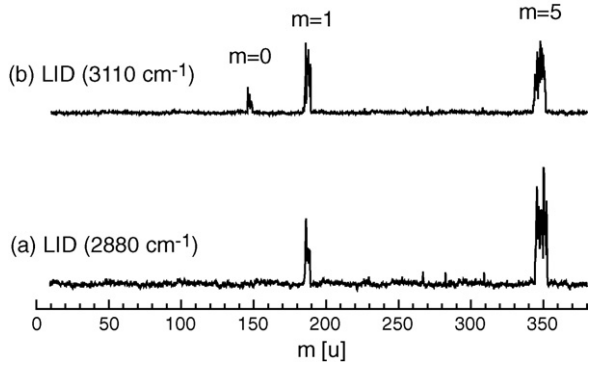

Fig. 6. Laser-induced dissociation (LID) mass spectra of $pDCB^+$–Ar_6 ($m=386$ u) for resonant excitation of the transitions B (a) and H (b) at 2880 and 3110 cm^{-1}, respectively. The mass spectra display fragmentation into $pDCB^+$–Ar_m with $m=5$ arising from metastable decay (MD) and $m=0$ and 1 arising from laser-induced dissociation (LID).

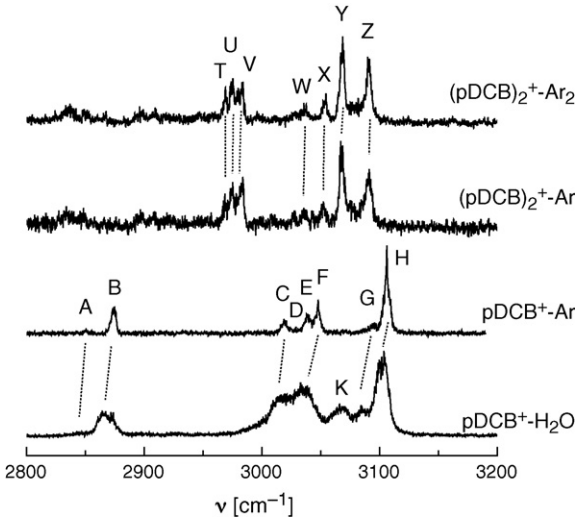

Fig. 7. IRPD spectra of $pDCB^+–H_2O$, $pDCB^+$–Ar, $(pDCB)_2^+$–Ar, and $(pDCB)_2^+–Ar_2$ in the C–H stretch range recorded in the $pDCB^+$ or $(pDCB)_2^+$ fragment channel. The positions and assignments of the transitions observed (A–H, T–Z) are listed in Tables 1 and 5.

per Ar ligand, a value which is consistent with the dissociation energy of $577\,cm^{-1} < D_0 < 656\,cm^{-1}$ for $pDCB^+$–Ar determined by MATI spectroscopy [67]. Due to noncooperative three-body induction interactions, the Ar binding energy is expected to slightly decrease for increasing number of Ar ligands occupying roughly equivalent binding sites in the first solvation shell around an ionic core [11,68,87–89].

3.1.2. $pDCB^+–H_2O$

Fig. 7 compares the IRPD spectrum of $pDCB^+$–Ar with that of $pDCB^+–H_2O$ reported previously [21]. While the Ar ligand binds to the aromatic π electron system via dispersion and polarization forces with a dissociation energy of $\sim 550\,cm^{-1}$, the H_2O ligand binds via much stronger charge-dipole forces to the $pDCB^+$ cation ($\sim 2500\,cm^{-1}$) [21]. Due to their higher binding energy, the $pDCB^+–H_2O$ complexes generated in the electron impact ion source can possess more internal energy leading to broader transitions in the IR spectra, with widths of $\sim 15\,cm^{-1}$. Moreover, the transitions are similar in intensity and frequency but systematically redshifted compared to those of $pDCB^+$–Ar by 5–15 cm^{-1}. This effect is again attributed to the higher internal temperature of the $pDCB^+–H_2O$ complexes, which gives rise to sequence hot bands occurring to slightly lower frequency as the fundamental frequencies. The only transition in the $pDCB^+–H_2O$ spectrum, which does not have an obvious counterpart in the $pDCB^+$–Ar spectrum, is band K at $3065\,cm^{-1}$. It is not due to the overtone of the H_2O bend vibration, which occurs at $3152\,cm^{-1}$ for bare H_2O [90] and is predicted to be blueshifted by complexation with $pDCB^+$ [21].

Two $pDCB^+–H_2O$ isomers with charge-dipole bonding and C_{2v} symmetry were predicted at the B3LYP level [21]. In the H-bonded isomer (Fig. 1e), the lone pairs of the O atom of H_2O bind to H atoms of two adjacent CH groups of $pDCB^+$, whereas in the π-bonded isomer (Fig. 1d), the O atom interacts with the π-electron system. At the B3LYP level, the H-bonded isomer is slightly more stable than the π-bonded one, $D_0 = 2525$ and $2018\,cm^{-1}$ [21]. This energy difference obtained at $T = 0$ K is similar to the corresponding free energy difference obtained for $T = 300$ K, implying that entropy does not affect the energetic order of the two isomers. As both isomers have similar IR spectra in the O–H stretch range, they could not be distinguished by comparison with the experimental spectrum reported previously [21]. Also the C–H stretch frequencies are rather similar for both isomers [21]. However, the IR intensity of ν_{18} (band H) of the H-bonded isomer is predicted to be enhanced by a factor of 2.5 upon H-bonding, while the one of the π-bonded isomer is reduced by 25% [21]. As band H in the IR spectrum of $pDCB^+–H_2O$ has a slightly lower relative intensity than all the other bands when compared to the $pDCB^+$–Ar spectrum, it is likely that the π-bonded isomer is the dominant carrier of the $pDCB^+–H_2O$ spectrum, although it is calculated to be slightly less stable.

Table 5
Positions (in cm^{-1}) of the transitions observed in the IR spectra of $(pDCB)_2^+–Ar_n$ (Fig. 7).

	T	U	V	W	X	Y	Z
$n=1$	2969	2973	2984	3035	3052	3067	3091
$n=2$	2969	2975	2983	3036	3054	3067	3090

3.1.3. $(pDCB)_2^+–Ar_n$

Fig. 7 compares the IRPD spectra of $(pDCB)_2^+–Ar_n$ with $n = 1$ and 2 in the C–H stretch range. Both spectra look very similar, suggesting that Ar complexation has essentially no impact on the appearance of the IR spectrum of bare $(pDCB)_2^+$ in this spectral range. On the other hand, the $(pDCB)_2^+$ spectrum is rather different from those of pDCB and $pDCB^+$, which is ascribed to a charge-resonance structure of the dimer (*vide infra*). The transitions observed in the spectra of $(pDCB)_2^+–Ar_n$ are labeled T–Z, and their frequencies are collected in Table 5.

A variety of starting geometries have been used to locate minima on the $(pDCB)_2^+$ potential, and only symmetric dimer structures with equivalent pDCB units were obtained. The by far most stable structures located have charge-resonance geometries. The lowest energy isomer found has a parallel-displaced structure with C_{2h} symmetry and a binding energy of $D_0 = 3904\,cm^{-1}$ (Fig. 1f). In this isomer, the nearly planar pDCB molecules are separated by 3.5 Å and one Cl atom of one ring interacts with the π electron system of the other ring. The parallel sandwich structure (Fig. 1 g) is similar to that of $(Bz)_2^+$ [54,55]. It has a larger separation (3.8 Å) and smaller binding energy ($D_0 = 3617\,cm^{-1}$) than the parallel-displaced isomer, probably due to Cl. . .Cl repulsion of the large Cl atoms [59]. A sandwich dimer with the two rings rotated by 60° with respect to each other around the ring axis, as found for $(pDFB)_2^+$ [59], could not be obtained for $(pDCB)_2^+$ at the B3LYP/6-311++G** level. The calculated binding energies of 0.48 and 0.45 eV for the two $(pDCB)_2^+$ isomers are somewhat lower than those derived for $(Bz)_2^+$ (0.65–0.9 eV [54,60–62]) and $(pDFB)_2^+$ (0.7 eV [58]), possibly as a result of the displacement and/or the steric hindrance of the two rings. However, the $(pDCB)_2^+$ interaction is in both $(pDCB)_2^+$ dimers still significantly stronger than the strong ion–dipole bonds in the $pDCB^+–H_2O$ isomers (Fig. 1), again confirming the existence of the charge-resonance in the former complexes. In general, all geometric parameters of the pDCB moieties in $(pDCB)_2^+$ are between those of pDCB and $pDCB^+$ (Table 2), as expected for a charge-resonance structure in which both units carry half of the positive charge. As the spectra of $(pDCB)_2^+–Ar_n$ with $n = 1$ and 2 are quite similar, the weak interaction with Ar is insufficient to break the symmetry of $(pDCB)_2^+$ and to localize a significant amount of positive charge asymmetrically on one of the two pDCB units.

The charge-resonance has a drastic effect on the calculated IR spectrum of $(pDCB)_2^+$, which differs dramatically from those of pDCB and $pDCB^+$ with respect to both the vibrational frequencies and the IR intensities, in particular in the fingerprint range (see Fig. F1 in Supporting Information). This theoretical prediction is confirmed by the large differences in the experimental IR spectra of pDCB, $pDCB^+(–Ar_n)$, and $(pDCB)_2^+(–Ar_n)$ shown in Figs. 5 and 7. The $(pDCB)_2^+$ spectrum is not simply derived from an approximate addition of those of pDCB and $pDCB^+$, again confirming the charge-resonance structure of the dimer. For example, the bands

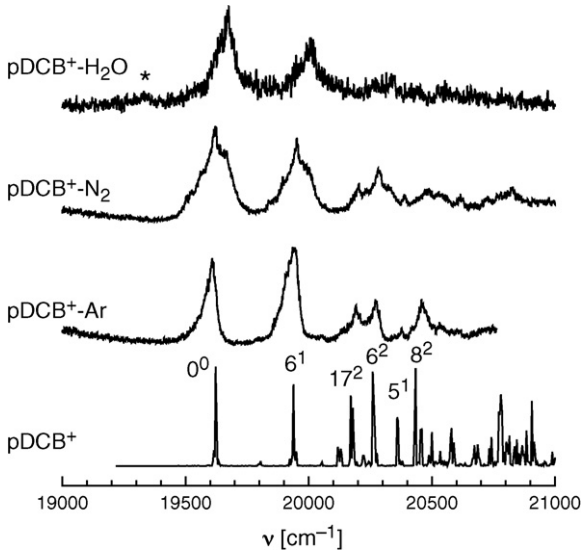

Fig. 8. Electronic photodissociation spectra of the B ← X transition of $pDCB^+$–Ar, $pDCB^+$–N_2, and $pDCB^+$–H_2O [21] monitored in the $pDCB^+$ channel compared to the corresponding spectrum of bare $pDCB^+$ recorded in the Cl loss channel in a cryogenic ion trap (10 K) [63]. The asterisk indicates a hot band assigned to ν_6.

T–V of $(pDCB)_2^+$–Ar_n near 2970 cm^{-1} are not visible in the spectra of $pDCB^+$–Ar_n and pDCB in the same spectral range. Similar to pDCB and $pDCB^+$, the IR spectrum of $(pDCB)_2^+$ is complicated by combination bands occurring in the C–H stretch range, and a reliable interpretation of the bands T–Z is not available at the present stage. Possibly, band Z corresponds to the symmetric linear combination of the ν_{18} C–H stretch fundamentals of the two pDCB units. The experimental redshift of the order of 15 cm^{-1} from the corresponding band of $pDCB^+$ (band H) is larger than those of 3–4 cm^{-1} predicted for the two $(pDCB)_2^+$ isomers (Fig. F1). The firm assignment of the other bands has to await a sophisticated anharmonic vibrational calculation [82], which is able to predict anharmonic frequencies and IR intensities of combination bands and overtones.

3.2. Electronic spectra

The vibronic spectra of the B $^2B_{3u}$ ← X $^2B_{2g}$ electronic transition of $pDCB^+$–L with L = Ar, N_2, and H_2O [21] are compared in Fig. 8 with the corresponding spectrum of the $pDCB^+$ monomer recorded in a cryogenic ion trap (at 10 K) [63]. The transitions observed are listed in Table 6, along with the vibrational assignment taken from Ref. [63]. The similar appearance of all spectra readily facilitates the assignment and demonstrates that complexation has little impact on the electronic and intramolecular vibrational properties of $pDCB^+$ in the $^2B_{3u}$ electronic state. The overall intramolecular structure of the B ← X transition is dominated by a progression in the ν_6 mode (~330 cm^{-1}, symmetric σ_{CCl}) and the ν_5 fundamental, which is consistent with the geometry change predicted for promotion of an electron from the lone pair of Cl to the aromatic π orbital.

In general, the widths of the transitions in the $pDCB^+$–L dimer spectra (~60, 130, and 80 cm^{-1} for the 0^0 band of L = Ar, N_2, and H_2O) in Fig. 8 are much larger than those observed in the $pDCB^+$ spectrum (~10 cm^{-1}) for several reasons. First, the (ro)vibrational temperatures of the $pDCB^+$–L dimers generated in the EI source are much higher than that of $pDCB^+$ in the 10 K trap. As the binding energy rises in the order Ar < N_2 < H_2O, the degree of internal excitation increases in the same order [25]. This conclusion is supported by the hot band assigned to ν_6 (~330 cm^{-1}) in the $pDCB^+$–H_2O spectrum (Fig. 8), which indicates a vibrational temperature of ~200 K [21]. Table 3 illustrates that $pDCB^+$ has in total six modes in the ground state with frequencies below 400 cm^{-1}, which may all contribute to the width via unresolved sequence hot bands. A further contribution to the width comes from unresolved intermolecular vibrational structure. The three, five, and six intermolecular modes of $pDCB^+$–L with L = Ar, N_2, and H_2O have calculated frequencies below 60, 100, and 400 cm^{-1}, respectively. The $pDCB^+$–N_2 structure obtained at the B3LYP level adopts a π-bonded charge–quadrupole configuration, in which the N_2 ligands approaches the C atom with the Cl substituent in a linear fashion at a separation of 3.6 Å. Such an approach is favored by the anisotropy of the electrostatic charge–quadrupole interaction as well as the charge-induced dipole forces, which dominate the attraction in this complex at long range [32,78,91]. The calculated binding energy of 173 cm^{-1} is much lower than the values measured for related complexes (500–1000 cm^{-1} [78]), confirming that the B3LYP level does not reliably describe the interaction strength in this complex.

Due to the broadening arising from spectral congestion, it is difficult to extract the exact positions of the 0^0 bands of the $pDCB^+$–L dimers. The values in Table 6 correspond to the maxima of the bands, and the complexation-induced shifts of $\Delta = -16$, -1, and $+51$ cm^{-1} derived in this way are only accurate to within 50 cm^{-1}. In any case, these shifts are minor compared to the dissociation energies of the complexes (Fig. 1), indicating that electronic excitation has only a minor effect on the intermolecular binding energy. Although the 0^0 bands of $pDCB^+$–Ar and $pDCB^+$–N_2 display some reproducible regular structure, which may be assigned to progressions of low-frequency intermolecular modes of the π-bonded complexes, the resolution of the spectra is insufficient for a detailed analysis. However, the progressions are relatively short, suggesting that the intermolecular geometry change induced upon electronic excitation is not substantial. Thus, the intermolecular interaction potential of all three dimers is hardly affected by electronic excitation, with respect to both the interaction energy and the equilibrium geometry. This situation is similar to electronic excitation of neutral pDCB–Ar and as well as ionization to the ground electronic state [67]. Interestingly, the redshift of the 0^0 band of the B ← X transition of $pDCB^+$ induced by an Ar matrix is $\Delta = -410$ cm^{-1} [92], i.e. much larger than that generated by a single Ar ligand. This is expected, as further Ar ligands added to the first solvation shell around the $pDCB^+$ core ion will cause additional redshifts of similar magnitude.

The electronic spectrum of $(pDCB)_2^+$ in the spectral range 19,000–21,000 cm^{-1} did not show any resolved structure on top of a broad continuum. This is consistent with the charge-resonance interaction of the homodimer predicted by the calculations, which is supposed to induce large shifts in the electronic transitions [37,58]. As the ionization energies [53] of the ligands L = Ar (15.8 eV), N_2 (15.6 eV), and H_2O (12.6 eV) are well above that of pDCB (8.9 eV), the positive charge in these $pDCB^+$–L dimers is well localized on the aromatic molecule, in line with the natural bond

Table 6
Maxima of the vibronic transitions (in cm^{-1}) in the excitation spectra the B $^2B_{3u}$ ← X $^2B_{2g}$ electronic transition of $pDCB^+$–L with L = Ar, N_2, and H_2O compared the those of bare $pDCB^+$ (Fig. 8).

Peaks	$pDCB^+$[a]	$pDCB^+$[b]	$pDCB^+$–Ar	$pDCB^+$–N_2	$pDCB^+$–H_2O
0^0	19,622 ± 2	19,212 ± 12	19,606	19,621	19,673
Δ	0	−410	−16[c]	−1[c]	+51[c]
ν_6	+320	+331	+338	+330	+335
$2\nu_{17}$	+553		+584	+582	+595
$2\nu_6$	+638	+637	+665	+661	+666
ν_5	+737		+768	+766	+759
$2\nu_8$	+812		+851	+867	+879

[a] Gas phase at 10 K [63].
[b] From Ar matrix data (12 K) [46].
[c] Uncertainty ±50 cm^{-1} (see text).

orbital analysis yielding positive charges of less than 0.02 e on the ligands in $pDCB^+$–L. As the $pDCB^+$ ion acts as the chromophore of the $B \leftarrow X$ transition of $pDCB^+$–L, the transition energies are only slightly perturbed. On the other hand, the positive charge is completely delocalized over the dimer in $(pDCB)_2^+$, leading to a substantial perturbation of the electronic structure and the resulting excitation spectrum, as well as a much stronger intermolecular bond.

4. Concluding remarks

IR and electronic excitation spectra of clusters of $pDCB^+$ have been obtained by vibrational and electronic photodissociation spectroscopy. The IR spectra of $pDCB^+$–Ar_n and $(pDCB)_2^+$–Ar_n in the C–H stretch range of the ground electronic state display essentially no shift as a function of the Ar cluster size and approximate to high accuracy the hitherto unknown IR spectra of $pDCB^+$ and its $(pDCB)_2^+$ homodimer (messenger technique [19,24,26,73,93]). In addition to the two IR active C–H stretch fundamentals of $pDCB^+$, several intense combination bands are detected and assigned in the 2800–3100 cm^{-1} range via a detailed analysis of the structural and vibrational properties of pDCB and $pDCB^+$ employing B3LYP/6-311++G** calculations. This analysis yielded a reassignment of two of the four IR modes known so far. The bond dissociation energy of ~550 cm^{-1} for π-bonded $pDCB^+$–Ar estimated from the photofragmentation data is consistent with the value determined previously by MATI spectroscopy. The IR spectrum of $pDCB^+$–H_2O in the C–H stretch range supports a π-bonded charge–dipole structure with a dissociation energy of ~2000 cm^{-1}. The analysis of the IR spectrum of $(pDCB)_2^+$, as inferred from the spectrum of Ar-tagged species is indicative of a charge-resonance type interaction typical for nonhydrogen-bonded aromatic homodimer cations. The electronic spectra of the $B\ ^2B_{3u} \leftarrow X\ ^2B_{2g}$ transition of $pDCB^+$–L with L = Ar, N_2, and H_2O near 500 nm display only small complexation shifts, suggesting little change in the geometry and binding energy of the intermolecular interaction upon electronic excitation. The lack of a structured spectrum for $(pDCB)_2^+$ in this spectral range confirms the charge-resonance geometry for this aromatic homodimer. Future efforts aim at the search of the electronic spectrum of $(pDCB)_2^+$ using a broadly tunable UV/vis OPO laser. Furthermore, sophisticated vibrational calculations [82] are envisaged to predict reliable anharmonic frequencies and IR intensities of overtone and combination bands of $pDCB^+$ and $(pDCB)_2^+$, which are required for a detailed interpretation of the experimental IR spectra and a fundamental understanding of the effects of the charge-resonance on the vibrational spectrum of aromatic homodimers.

Acknowledgments

This study was supported by the *Deutsche Forschungsgemeinschaft* (DO 729/2 and 729/4) and the *Fonds der Chemischen Industrie*. We thank E.J. Bieske (Melbourne) for providing the electronic spectrum of $pDCB^+$.

Appendix A. Supplementary data

Supplementary data associated with this article can be found, in the online version, at doi:10.1016/j.ijms.2010.06.026.

References

[1] E.A. Meyer, R.K. Castellano, F. Diederich, Angew. Chem. Int. Ed. 42 (2003) 1210.
[2] R. Leist, J.A. Frey, P. Ottiger, H.M. Frey, S. Leutwyler, R.A. Bachorz, W. Klopper, Angew. Chem. Int. Ed. 46 (2007) 7449.
[3] K. Mizuse, H. Hasegawa, N. Mikami, A. Fujii, J. Phys. Chem. A, J. Phys. Chem. A, in press, doi:10.1021/jp1009466.
[4] B. Brutschy, Chem. Rev. 100 (2000) 3891.
[5] C.E.H. Dessent, K. Müller-Dethlefs, Chem. Rev. 100 (2000) 3999.
[6] T. Ebata, A. Fujii, N. Mikami, Int. Rev. Phys. Chem. 17 (1998) 331.
[7] K. Müller-Dethlefs, O. Dopfer, T.G. Wright, Chem. Rev. 94 (1994) 1845.
[8] H.J. Neusser, H. Krause, Chem. Rev. 94 (1994) 1829.
[9] K. Kleinermanns, M. Gerhards, M. Schmitt, Ber. Bunsenges. Phys. Chem. 101 (1997) 1785.
[10] B. Brutschy, Chem. Rev. 92 (1992) 1567.
[11] O. Dopfer, Z. Phys. Chem. 219 (2005) 125.
[12] S. Ishiuchi, M. Sakai, Y. Tsuchida, A. Takeda, Y. Kawashima, M. Fujii, O. Dopfer, K. Müller-Dethlefs, Angew. Chem. Int. Ed. 44 (2005) 6149.
[13] K. Kleinermanns, C. Janzen, D. Spangenberg, M. Gerhards, J. Phys. Chem. A 103 (1999) 5232.
[14] H. Piest, G. von Helden, G. Meijer, J. Chem. Phys. 110 (1999) 2010.
[15] T. Pino, N. Boudin, P. Brechignac, J. Chem. Phys. 111 (1999) 7337.
[16] N. Gonohe, H. Abe, N. Mikami, M. Ito, J. Phys. Chem. 89 (1985) 3642.
[17] Y. Inokuchi, N. Nishi, J. Chem. Phys. 114 (2001) 7059.
[18] M. Miyazaki, A. Fujii, T. Ebata, N. Mikami, Phys. Chem. Chem. Phys. 5 (2003) 1137.
[19] G.E. Douberly, A.M. Ricks, P.V.R. Schleyer, M.A. Duncan, J. Phys. Chem. A 112 (2008) 4869.
[20] K. Mizuse, A. Fujii, N. Mikami, J. Phys. Chem. A 110 (2006) 6387.
[21] S. Chakraborty, A. Patzer, A. Lagutschenkov, J. Langer, O. Dopfer, Chem. Phys. Lett. 485 (2010) 49.
[22] M. Miyazaki, A. Fujii, T. Ebata, N. Mikami, Chem. Phys. Lett. 349 (2001) 431.
[23] M. Miyazaki, A. Fujii, T. Ebata, N. Mikami, J. Phys. Chem. A 108 (2004) 10656.
[24] A. Fujii, E. Fujimaki, T. Ebata, N. Mikami, J. Chem. Phys. 112 (2000) 6275.
[25] N. Solcà, O. Dopfer, Chem. Phys. Lett. 347 (2001) 59.
[26] O. Dopfer, R.V. Olkhov, J.P. Maier, J. Chem. Phys. 111 (1999) 10754.
[27] N. Solcà, O. Dopfer, Chem. Phys. Lett. 325 (2000) 354.
[28] A. Patzer, H. Knorke, J. Langer, O. Dopfer, Chem. Phys. Lett. 457 (2008) 298.
[29] A. Takeda, H.S. Andrei, M. Miyazaki, S.I. Ishiuchi, M. Sakai, M. Fujii, O. Dopfer, Chem. Phys. Lett. 443 (2007) 227.
[30] N. Solcà, O. Dopfer, J. Phys. Chem. A 105 (2001) 5637.
[31] N. Solcà, O. Dopfer, Eur. Phys. J. D 20 (2002) 469.
[32] N. Solcà, O. Dopfer, J. Phys. Chem. A 106 (2002) 7261.
[33] U. Lorenz, N. Solcà, O. Dopfer, Chem. Phys. Lett. 406 (2005) 321.
[34] H.S. Andrei, N. Solca, O. Dopfer, Phys. Chem. Chem. Phys. 6 (2004) 3801.
[35] H.S. Andrei, N. Solca, O. Dopfer, J. Phys. Chem. A 109 (2005) 3598.
[36] N. Solcà, O. Dopfer, Phys. Chem. Chem. Phys. 6 (2004) 2732.
[37] Y. Nakai, K. Ohashi, N. Nishi, J. Phys. Chem. A 101 (1997) 472.
[38] T. Pino, S. Douin, N. Boudin, P. Brechignac, Chem. Phys. Lett. 419 (2006) 356.
[39] E.J. Bieske, J.P. Maier, Chem. Rev. 93 (1993) 2603.
[40] E.J. Bieske, M.W. Rainbird, A.E.W. Knight, J. Phys. Chem. 94 (1990) 3962.
[41] N. Mikami, T. Sasaki, S. Sato, Chem. Phys. Lett. 180 (1991) 431.
[42] M. Miyazaki, A. Fujii, T. Ebata, N. Mikami, Chem. Phys. Lett. 399 (2004) 412.
[43] N. Solcà, O. Dopfer, J. Phys. Chem. A 107 (2003) 4046.
[44] N. Solcà, O. Dopfer, Chem. Phys. Chem. 6 (2005) 434.
[45] N. Solcà, O. Dopfer, J. Am. Chem. Soc. 125 (2003) 1421.
[46] J. Szczepanski, W. Personette, R. Pellow, T.M. Chandrasekhar, D. Roser, M. Cory, M. Zerner, M. Vala, J. Chem. Phys. 96 (1992) 35.
[47] T. Kato, N. Muraki, T. Shida, Chem. Phys. Lett. 164 (1989) 388.
[48] A. Gaber, M. Riese, J. Grotemeyer, Phys. Chem. Chem. Phys. 10 (2008) 1168.
[49] C. Garrigou-Lagrange, J.M. Lebas, M.L. Josien, Spectrochim. Acta 12 (1958) 305.
[50] J.M. Lebas, C. Garrigoulagrange, M.L. Josien, Spectrochim. Acta 15 (1959) 225.
[51] A. Stojiljkovic, D.H. Whiffen, Spectrochim. Acta 12 (1958) 47.
[52] J.R. Scherer, J.C. Evans, Spectrochim. Acta 19 (1963) 1739.
[53] P.J. Linstrom, W.G. Mallard, NIST Chemistry WebBook, NIST Standards and Technology, Gaithersburg, MD 20899, 2001, http://webbook.nist.gov.
[54] P.A. Pieniazek, S.E. Bradforth, A.I. Krylov, J. Chem. Phys. 129 (2008) 074104.
[55] Y. Itagaki, N.P. Benetis, R.M. Kadam, A. Lund, Phys. Chem. Chem. Phys. 2 (2000) 2683.
[56] P.A. Pieniazek, A.I. Krylov, S.E. Bradforth, J. Chem. Phys. 127 (2007) 044317.
[57] O. Dopfer, G. Lembach, T.G. Wright, K. Müller-Dethlefs, J. Chem. Phys. 98 (1993) 1933.
[58] Y.H. Hu, M.X. Liu, X.J. Wang, J.Y. Zhou, X. Yang, S.H. Yang, Acta Phys.-Chim. Sin. 15 (1999) 1057.
[59] Y. Itagaki, N. Yanagida, M. Shiotani, Phys. Chem. Chem. Phys. 4 (2002) 5982.
[60] Y. Ibrahim, E. Alsharaeh, M. Rusyniak, S. Watson, M.M.N. Mautner, M.S. El-Shall, Chem. Phys. Lett. 380 (2003) 21.
[61] K. Hiraoka, S. Fujimaki, K. Aruga, S. Yamabe, J. Chem. Phys. 95 (1991) 8413.
[62] J.R. Grover, E.A. Walters, E.T. Hui, J. Phys. Chem. 91 (1987) 3233.
[63] A. Dzhonson, D. Gerlich, E.J. Bieske, J.P. Maier, J. Mol. Struct. 795 (2006) 93.
[64] A. Gaber, M. Riese, J. Grotemeyer, J. Phys. Chem. A 112 (2008) 425.
[65] B. Ruscic, L. Klasinc, A. Wolf, J.V. Knop, J. Phys. Chem. 85 (1981) 1486.
[66] S.Y. Yu, M.B. Huang, J. Mol. Struct. Theochem. 822 (2007) 48.
[67] A. Gaber, M. Riese, F. Witte, J. Grotemeyer, Phys. Chem. Chem. Phys. 11 (2009) 1628.
[68] O. Dopfer, Int. Rev. Phys. Chem. 22 (2003) 437.
[69] F. Muntean, L. Heumann, P.B. Armentrout, J. Chem. Phys. 116 (2002) 5593.
[70] C. Camy-Peyret, J.M. Flaud, G. Guelachvili, C. Amiot, Mol. Phys. 26 (1973) 825.
[71] M.J. Frisch, G.W. Trucks, H.B. Schlegel, G.E. Scuseria, M.A. Robb, J.R. Cheeseman, J.A. Montgomery, T. Vreven, K.N. Kudin, J.C. Burant, J.M. Millam, S.S. Iyengar, J. Tomasi, V. Barone, B. Menucci, M. Cossi, G. Scalmani, N. Rega, G.A. Petersson, H. Nakatsuji, M. Hada, M. Ehara, K. Toyota, R. Fukuda, J. Hasegawa, M. Ishida, T. Nakajima, Y. Honda, O. Kitao, H. Nakai, M. Klene, X. Li, J.E. Knox, H.P. Hratchian, J.B. Cross, C. Adamo, J. Jaramillo, R. Gomperts, R.E. Stratman, O. Yazyev, A.J.

Austin, R. Cammi, C. Pomelli, J. Ochterski, P.Y. Ayala, K. Morokuma, G.A. Voth, P. Salvador, J.J. Dannenberg, V.G. Zakrzewski, S. Dapprich, A.D. Daniels, M.C. Strain, O. Farkas, D.K. Malick, D. Rabuck, K. Raghavachari, J.B. Foresman, J.V. Ortiz, Q. Cui, A.G. Baboul, S. Clifford, J. Cioslowski, B.B. Stefanov, G. Liu, A. Liashenko, P. Piskorz, I. Komaromi, R.L. Martin, D.J. Fox, T. Keith, M.A. Al-Laham, C.Y. Peng, A. Nanayakkara, M. Challacombe, P.M.W. Gill, B.G. Johnson, W. Chen, M.W. Wong, C. Gonzales, J.A. Pople, Gaussian 03, Revision C.02, Gaussian, Inc., Pittsburgh, PA, 2004.
[72] M.D. Halls, J. Velkovski, H.B. Schlegel, Theor. Chem. Acc. 105 (2001) 413.
[73] M. Okumura, L.I. Yeh, J.D. Myers, Y.T. Lee, J. Phys. Chem. 94 (1990) 3416.
[74] S.A. Nizkorodov, O. Dopfer, T. Ruchti, M. Meuwly, J.P. Maier, E.J. Bieske, J. Phys. Chem. 99 (1995) 17118.
[75] O. Dopfer, R.V. Olkhov, J.P. Maier, J. Phys. Chem. A 103 (1999) 2982.
[76] R.V. Olkhov, S.A. Nizkorodov, O. Dopfer, Chem. Phys. 239 (1998) 393.
[77] N. Solcà, O. Dopfer, Angew. Chem. Int. Ed. 41 (2002) 3628.
[78] N. Solcà, O. Dopfer, Chem. Eur. J. 9 (2003) 3154.
[79] N. Solcà, O. Dopfer, J. Am. Chem. Soc. 126 (2004) 1716.
[80] N. Solcà, O. Dopfer, Angew. Chem. Int. Ed. 42 (2003) 1537.
[81] N. Solcà, O. Dopfer, J. Chem. Phys. 121 (2004) 769.
[82] H.G. Kjaergaard, A.L. Garden, G.M. Chaban, R.B. Gerber, D.A. Matthews, J.F. Stanton, J. Phys. Chem. A 112 (2008) 4324.
[83] A.A. Adesokan, G.M. Chaban, O. Dopfer, R.B. Gerber, J. Phys. Chem. A 111 (2007) 7374.
[84] O. Dopfer, D. Roth, J.P. Maier, J. Phys. Chem. A 104 (2000) 11702.
[85] O. Dopfer, N. Solcà, R.V. Olkhov, J.P. Maier, Chem. Phys. 283 (2002) 85.
[86] O. Dopfer, D. Roth, J.P. Maier, Int. J. Mass. Spectrom. 218 (2002) 281.
[87] R.G. Keesee, A.W. Castleman Jr., J. Phys. Chem. Ref. Data 15 (1986) 1011.
[88] O. Dopfer, Chem. Phys. 283 (2002) 63.
[89] O. Dopfer, J. Phys. Chem. A 104 (2000) 11693.
[90] J.M. Flaud, C. Camy-Peyret, Mol. Phys. 26 (1973) 811.
[91] D. Roth, O. Dopfer, Phys. Chem. Chem. Phys. 4 (2002) 4855.
[92] R.S. Friedman, B.J. Kelsall, L. Andrews, J. Phys. Chem. 88 (1984) 1944.
[93] J.R. Roscioli, L.R. McCunn, M.A. Johnson, Science 316 (2007) 249.